

Article

Organo-Nanocups Assist the Formation of Ultra-Small Palladium Nanoparticle Catalysts for Hydrogen Evolution Reaction

Erik Biehler, Qui Quach, Clay Huff and Tarek M. Abdel-Fattah * 

Applied Research Center at Thomas Jefferson National Accelerator Facility and Department of Molecular Biology and Chemistry, Christopher Newport University, Newport News, VA 23606, USA; erik.biehler.16@cnu.edu (E.B.); qui.quach.13@cnu.edu (Q.Q.); clay.huff.12@cnu.edu (C.H.)

* Correspondence: fattah@cnu.edu

Abstract: Ultra-small palladium nanoparticles were synthesized and applied as catalysts for a hydrogen evolution reaction. The palladium metal precursor was produced via beta-cyclodextrin as organo-nanocup (ONC) capping agent to produce ultra-small nanoparticles used in this study. The produced ~3 nm nanoparticle catalyst was then characterized via X-ray diffraction (XRD), transmission electron microscopy (TEM), ultraviolet-visible spectroscopy (UV-Vis), and Fourier transform infrared spectroscopy (FTIR) to confirm the successful synthesis of ~3 nm palladium nanoparticles. The nanoparticles' catalytic ability was explored via the hydrolysis reaction of sodium borohydride. The palladium nanoparticle catalyst performed best at 303 K at a pH of 7 with 925 μmol of sodium borohydride having an H_2 generation rate of $1.431 \text{ mL min}^{-1} \text{ mL}_{\text{cat}}^{-1}$. The activation energy of the palladium catalyst was calculated to be 58.9 kJ/mol.

Keywords: palladium nanoparticles; organo-nanocups; catalysts; hydrogen evolution; hydride precursors



Citation: Biehler, E.; Quach, Q.; Huff, C.; Abdel-Fattah, T.M.

Organo-Nanocups Assist the Formation of Ultra-Small Palladium Nanoparticle Catalysts for Hydrogen Evolution Reaction. *Materials* **2022**, *15*, 2692. <https://doi.org/10.3390/ma15072692>

Academic Editors: Ilenia Rossetti and Simona Bennici

Received: 11 March 2022

Accepted: 2 April 2022

Published: 6 April 2022

Publisher's Note: MDPI stays neutral with regard to jurisdictional claims in published maps and institutional affiliations.



Copyright: © 2022 by the authors. Licensee MDPI, Basel, Switzerland. This article is an open access article distributed under the terms and conditions of the Creative Commons Attribution (CC BY) license (<https://creativecommons.org/licenses/by/4.0/>).

1. Introduction

Within the past 20 years, nanotechnology has allowed the development of smaller, more intricate systems and materials that have revolutionized many fields of study, including medicine, chemistry, and engineering. This has provided a great deal of positive change for numerous applications such as sensors, adsorbents, solar cells, and catalysis [1–9]. The unique properties of nanomaterials are ultimately driving their application in many fields, and their dimensions allow them to replace conventional materials to provide smaller, more efficient technologies [8–10]. This allows typically costly materials, such as precious metals, to be applied in economical ways with more efficient means, ultimately stretching global reserves further.

The transition metals, commonly known as precious metals or platinum group metals, have been prized for centuries due to their chemical resistivity caused by a full d-shell orbital. These metals are not only found in jewelry but also in many electrical and chemical applications due to their high conductivity and resistance to oxidation. Nanoparticles (NPs) of these precious metals, such as silver and gold, have shown impressive catalytic activity in hydrogenation and hydrogen evolution reactions [5,7,9–12]. Platinum and palladium NPs have also been used in a variety of organic reactions and have been studied in hydrogen evolution reactions [13–17]. Despite the high cost of these transition metals, nanoparticles of these elements are much less expensive than bulk and are more effective due to the innately high surface area to volume ratio of nanomaterials.

Hydrogen energy has been identified as a possible green alternative fuel source [18–20]. Due to the dangers and energy intensity of hydrogen gas storage, research has focused on producing the gas on an as-needed basis for fuel cells [21–23]. Sodium borohydride has been identified as a possible candidate for storing hydrogen gas for fuel cells due to its low

density and impressive hydrogen content of 10.8% wt. However, the hydrolysis reaction of aqueous NaBH_4 is slow and would require a catalyst to be effectively applied [21,24–26]. Gold and silver NPs have shown promise in the catalysis of this reaction in previous works, and palladium is known to be a strong catalyst for hydrogenation reactions from NaBH_4 [5,7,9,10,14–16,27].

In this study, we utilized beta-cyclodextrin as an organo-nanocup capping agent to synthesize and form a network of ultra-small palladium nanoparticles (PdNPs). The PdNPs were characterized by various methods * applied in catalyzing the hydrogen generation reactions under various temperatures, pH, and reactant concentrations. At 303 K, the PdNPs catalyzed reaction produced a highest hydrogen amount at pH of 7 with 925 μmol of sodium borohydride.

2. Experimental

2.1. Materials

Palladium (II) chloride (Sigma-Aldrich, St. Louis, MO, USA, 99.9%), beta-cyclodextrin (Sigma-Aldrich, 99%), sodium borohydride (J.T. Baker, Phillipsburg, NJ, USA, 98%), deionized water (18 M Ω).

2.2. Synthesis

A 1 mM solution of Palladium (II) chloride was first created. A separate solution of aqueous beta-cyclodextrin (β -CD) with a concentration of 10 mM was also made. These solutions were combined in a ratio by volume of 1:6.4 then stirred for approximately 10 min. A 180 mM solution of sodium borohydride (NaBH_4) was then made, chilled, and added to the above mixture in a 1:2 volume ratio. This mixture was then stirred for 120 min to aid in the formation of nanoparticle colloids (0.07 mM). All processes occurred at room temperature.

2.3. Characterization

The known identity of palladium nanoparticles was determined from the diffraction peaks seen using powder X-ray diffraction (XRD-Rigaku Miniflex II, Tokyo, Japan). The $\text{Cu K}\alpha$ X-ray was emitted from copper target tube. The $\text{Cu K}\beta$ radiation was filtered by nickel filters. The palladium nanoparticles were loaded on silicon wafer template and then scanned from 35° to 90°.

UV-Vis (Shimadzu UV-2600 UV-Vis Spectrophotometer, Kyoto, Japan) confirmed the successful reduction of Pd(II) to Pd(0).

Beta-cyclodextrin contains a major functional group that was identified using Fourier transform infrared spectroscopy (FTIR, Shimadzu IR-Tracer 100, Kyoto, Japan).

Transmission electron microscopy (TEM, JEM-2100F, JEOL Ltd., Akishima, Tokyo) helped characterize the nanoparticles produced by determining the dimensions of the nanoparticles and the electron diffraction patterns. We pipetted 1 μL of our catalyst onto a TEM grid and then dried it in an oven for 48 h prior to characterization.

2.4. Catalysis

Catalytic ability of our palladium nanoparticles was tested for evolution of hydrogen from aqueous sodium borohydride. The amount of hydrogen gas formed was quantified through the use of a gravimetric water displacement system [16,17]. The reactions of 625, 925, and 1225 μmol of aqueous NaBH_4 in 100 mL of deionized water were catalyzed using 200 μL of the palladium nanoparticle colloids (0.07 M). The catalytic activity was compared in varied temperature (283 K, 288 K, 295 K, 303 K) as well as varied pH (6, 7, 8) by manipulation of the reaction chamber using an ice bath or heating mantle for temperature trials and hydrochloric acid or sodium hydroxide for pH trials. The contents of the reaction chamber were stirred throughout the 120-min trials to maintain equal distribution of the catalyst and reactant in the solution. Throughout the catalytic activity tests, the reactions were run with 925 μmol of reactant in 0.1 L of deionized water with a temperature of 295 K

and a pH of 7 unless otherwise stated. The water displaced by the produced hydrogen gas was quantified with a Pioneer Balance (Pa124) made by Ohaus (Parsippany, NJ, USA) and using the SPDC Data Collector software (Ohaus, v2.01).

In the reusability test, 200 μL of palladium nanoparticles colloid was mixed with 100 mL of deionized water. Then 625 μmol of NaBH_4 was added to the above mixture. The reaction was run at pH 7 and a temperature of 295 K. After the reaction no longer produced more hydrogen, the same amount of NaBH_4 was added to test for the ability of palladium nanoparticles in continuing catalyzing the reactions.

3. Results and Discussion

3.1. Characterization

The UV-Vis Spectrum of PdNPs was displayed in Figure 1 and compared to that of PdCl_2 . The PdNPs showed absorbance peak at 315 nm, which was consistent with the absorbance range of previous studies [28,29]. The conversion of Pd(II) to Pd(0) was confirmed by the lack of the characteristic 415 nm peak [28–30]. These results confirmed the presence of PdNPs.

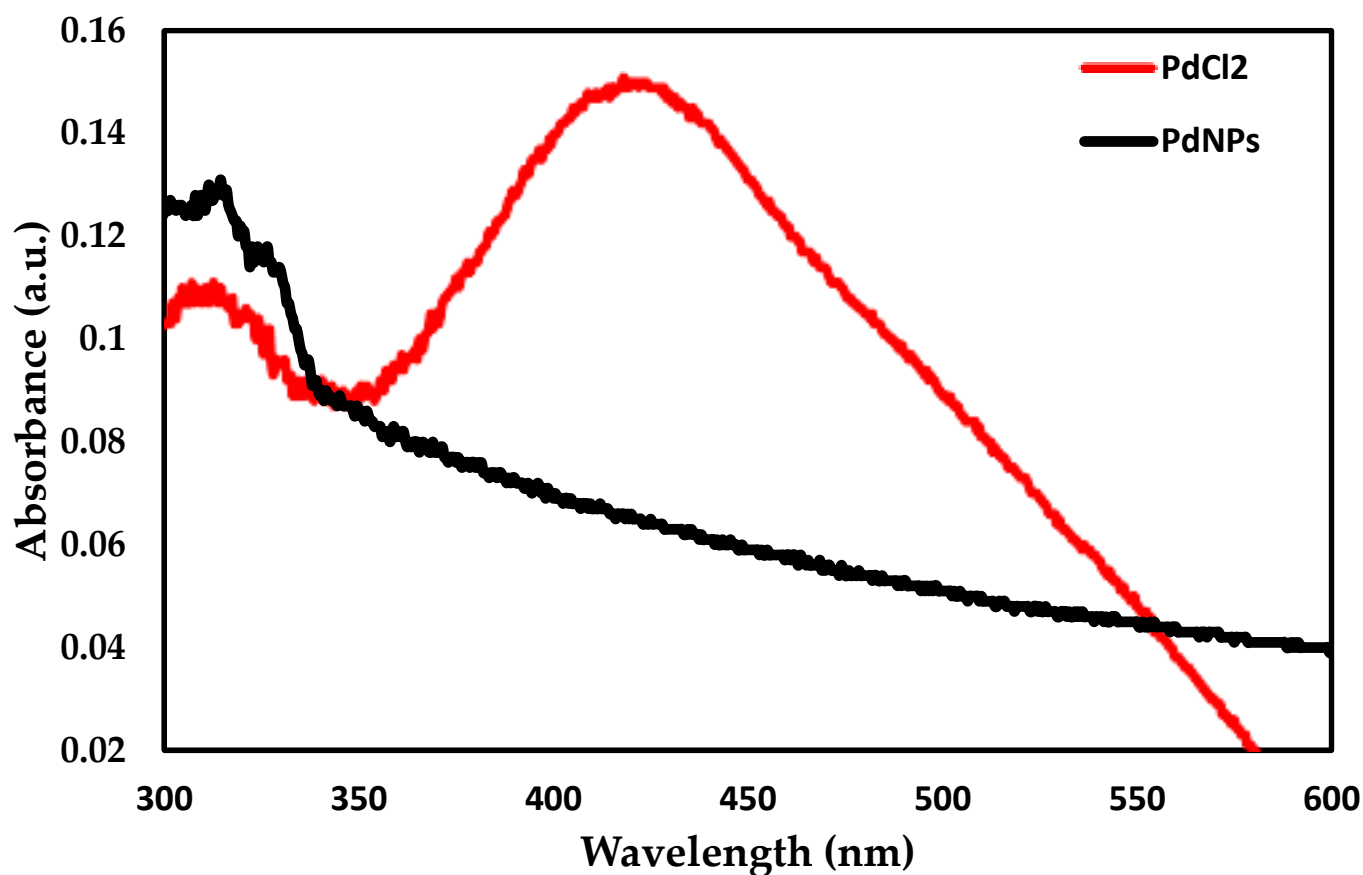


Figure 1. UV-Vis analysis of the spectra given off by PdNPs compared to that of PdCl_2 .

TEM micrographs (Figure 2) display the produced palladium nanoparticles (PdNPs). These images allowed the average diameter of our material to be determined to be 2.7 ± 0.8 nm. The TEM imaging again confirmed the successful synthesis of nanoparticles and showed that there was minimal agglomeration. Beta-cyclodextrin (Figure 3) as organo-nanocup (ONC) was used in conjunction with the nanoparticles to create a capping effect. The impressive uniformity of the produced nanoparticles combined with the facile nature of the synthesis makes beta-cyclodextrin an ideal capping agent to stabilize palladium nanoparticles.

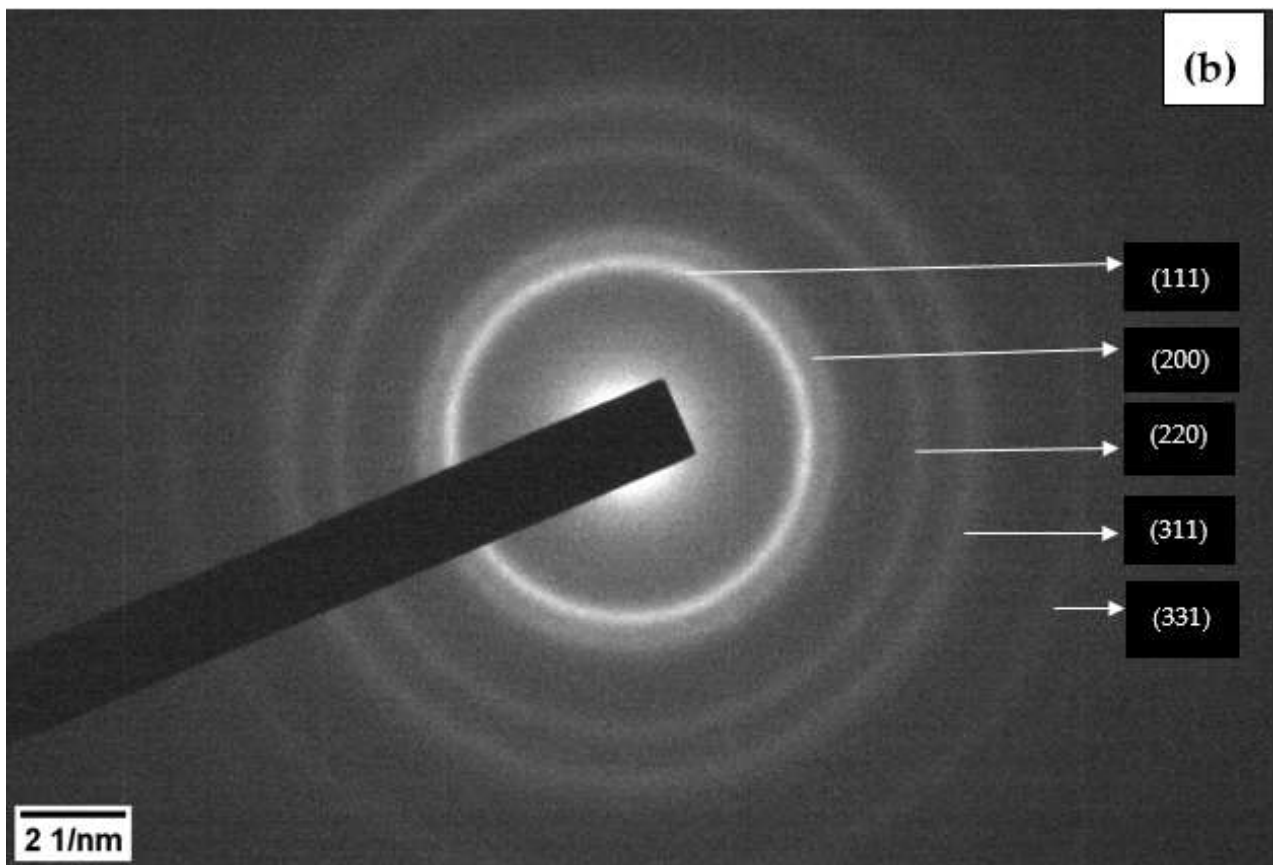
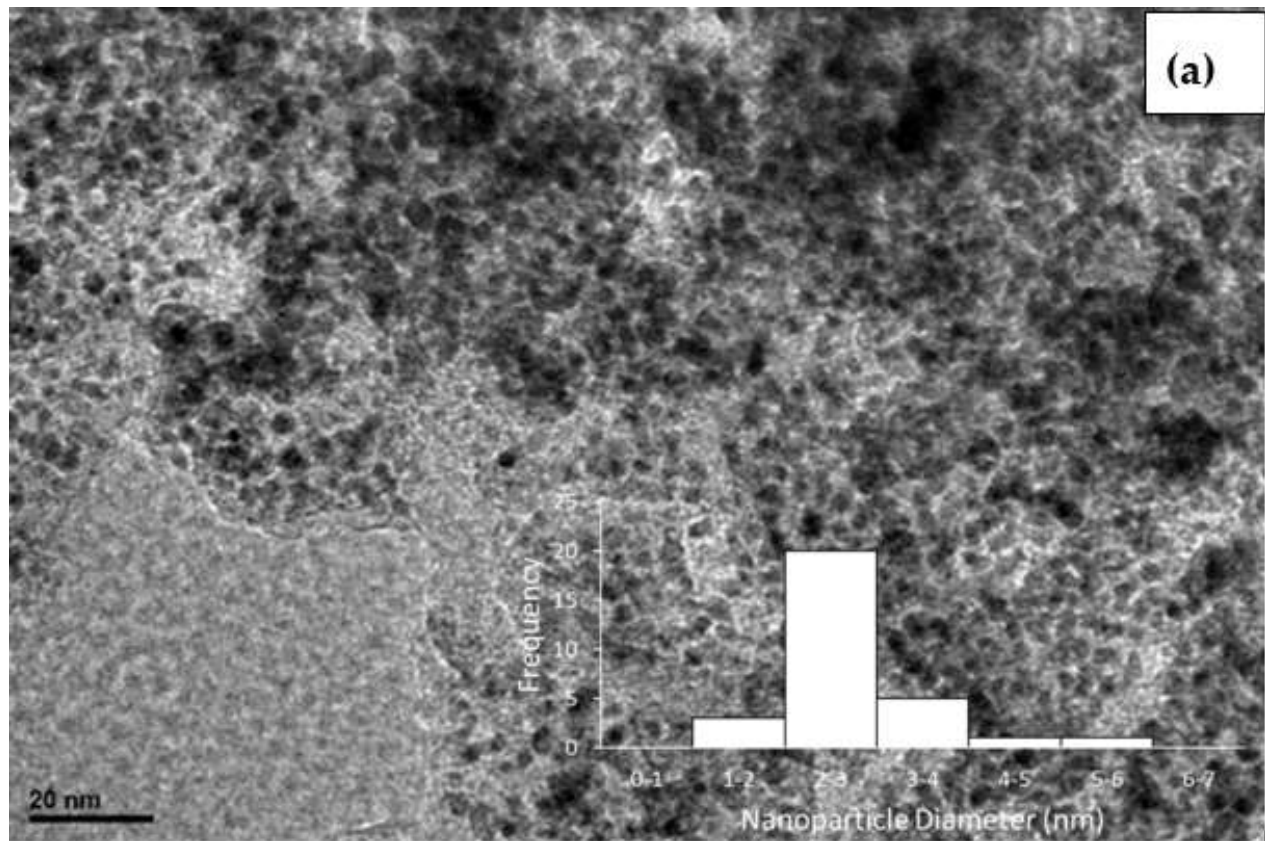


Figure 2. Cont.

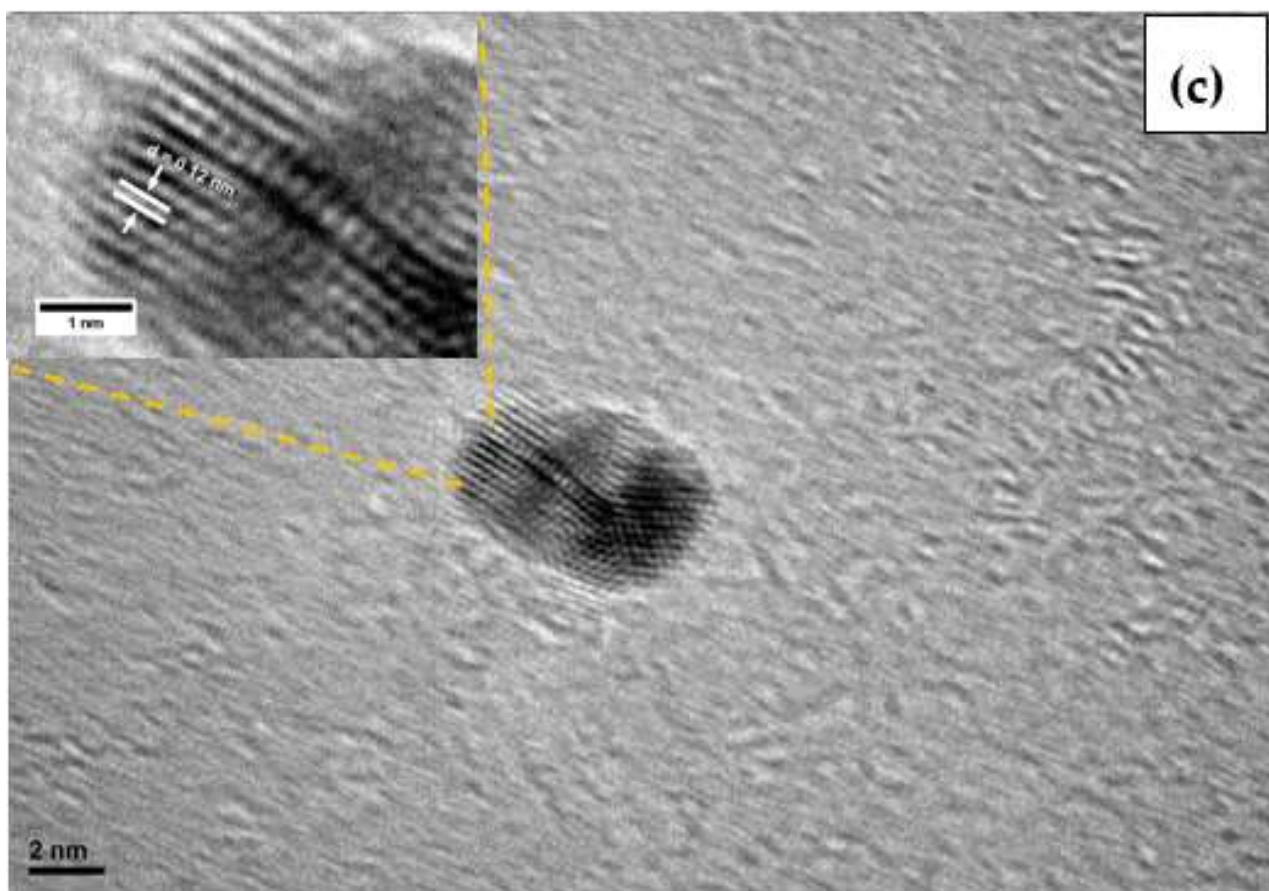


Figure 2. (a) Images of the palladium nanoparticles taken using TEM. The average diameter was determined to be 2.7 ± 0.8 nm. (b) The electron diffraction pattern of palladium nanoparticles. (c) Lattice fringes of palladium nanoparticles ($d = 0.12$ nm).

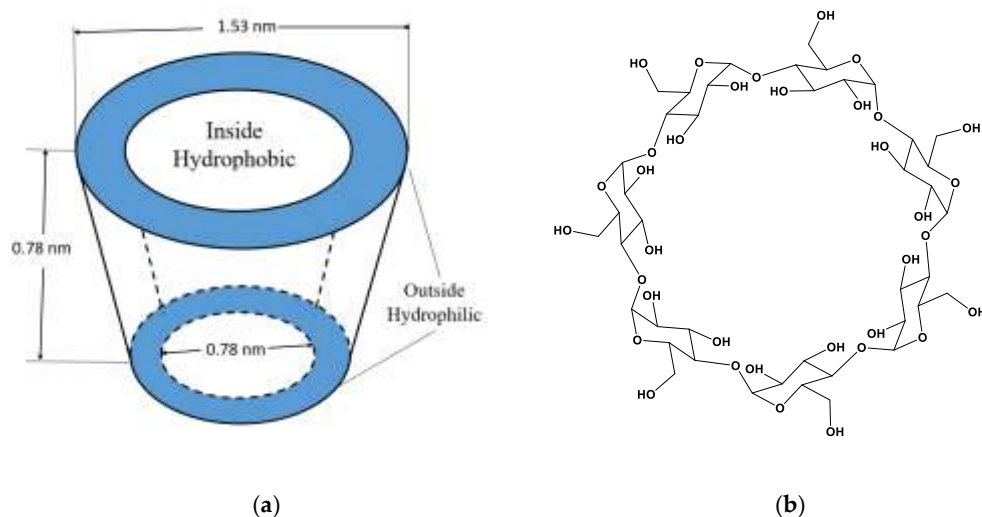


Figure 3. A graphical depiction of organo-nanocup capping agent of beta-cyclodextrin (a) and its molecular structure (b). Its shape consists of two hydroxyl rings, primary being the smaller of the two and secondary being the larger, and an internal cavity measuring 0.78 nm in diameter.

Beta-cyclodextrin's unique shape as nanocup aids in its efficiency as a capping agent [10]. The deep hydrophobic internal cavity in the center of the molecule confines nanoparticles within its narrow walls which prevents agglomeration by restricting their

ability to grow unchecked [10]. This effect results in isolated and uniform particles, which are more efficient catalysts due to their increased available surface area. The structure of beta-cyclodextrin was depicted in Figure 3. The outer diameter, inner diameter and height of beta-cyclodextrin were 1.53 nm, 0.78 nm and 0.78 nm, respectively [10,31].

The XRD pattern (Figure 4) displayed the crystallinity of the palladium nanoparticles. The peaks at 40° , 48° were corresponded with the (111) and (200) planes for a face centered cubic (FCC) of palladium nanoparticles [28–30]. The highest peak at 69° was attributed to the silicon wafer in which the nanoparticles are loaded on [32]. That the other planes of the palladium nanoparticles were not detected could be due to the size of the nanoparticles. It was indicated in the literature that the nanoparticles with the average size below 5 nm will influence the XRD pattern [33]. TEM electron diffraction (Figure 2b) confirmed the other planes of (220), (311), and (331) of palladium nanoparticles [34,35]. Figure 2c shows the lattice fringe of palladium nanoparticles in which the d spacing is 0.12 nm.

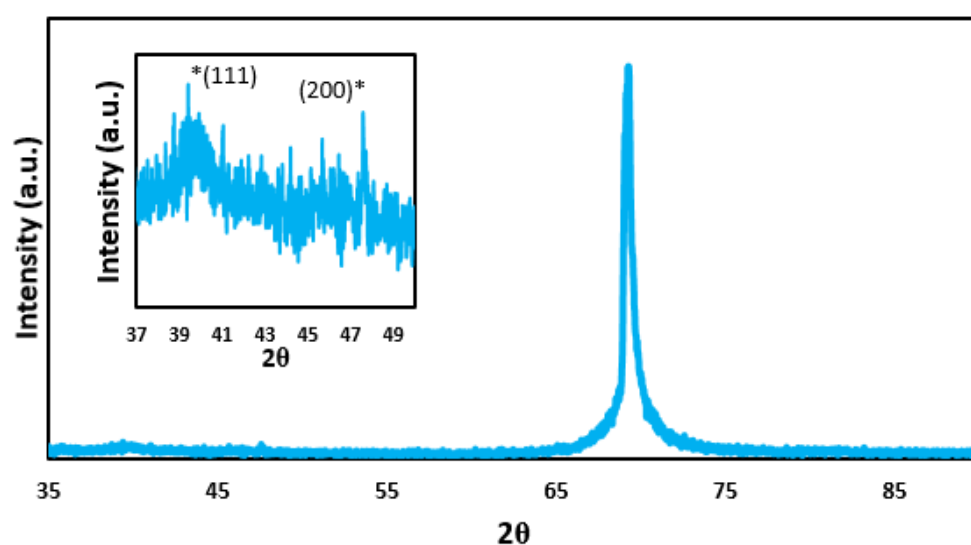


Figure 4. The characteristic peaks of the PdNPs on carbon tape from X-ray diffraction.

Supported β -CD in PdNPs was confirmed by FTIR (Figure 5). The IR spectrum showed characterized peaks at 1030 cm^{-1} , 1152 cm^{-1} and 1632 cm^{-1} that were corresponding with the vibrational stretching of glycosidic bond (C-O) of beta-cyclodextrin [36]. There was no strong peak at 2300 cm^{-1} , which indicated that no NaBH_4 remained in the nanoparticle colloids.

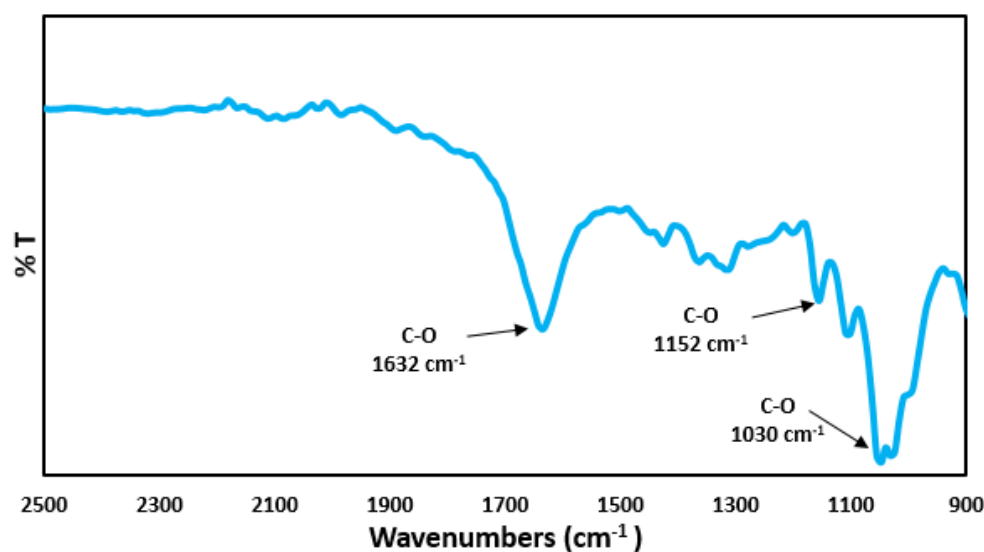


Figure 5. IR spectra of PdNPs.

3.2. Concentration Effect on Catalytic Ability

Under varied concentrations of reactants, the PdNPs showed the greatest hydrogen production rate of $1.194 \text{ mL min}^{-1} \text{ mL}_{\text{cat}}^{-1}$ with $1225 \mu\text{mol}$ of NaBH_4 (Figure 6). The next best conditions for the nanoparticle catalyst was $925 \mu\text{mol}$ for the PdNPs ($0.944 \text{ mL min}^{-1} \text{ mL}_{\text{cat}}^{-1}$). The lowest concentration for hydrogen production rate was $635 \mu\text{mol}$ of NaBH_4 producing H_2 gas at a rate of $0.650 \text{ mL min}^{-1} \text{ mL}_{\text{cat}}^{-1}$. Based on Figure 6 it is clear that there is a direct relationship between the concentration of NaBH_4 used in the reaction and the amount of hydrogen produced. This agrees with Le Chatelier's principle and Equation (1), where an increase in the reactants results in a shift to the right, increasing the products.

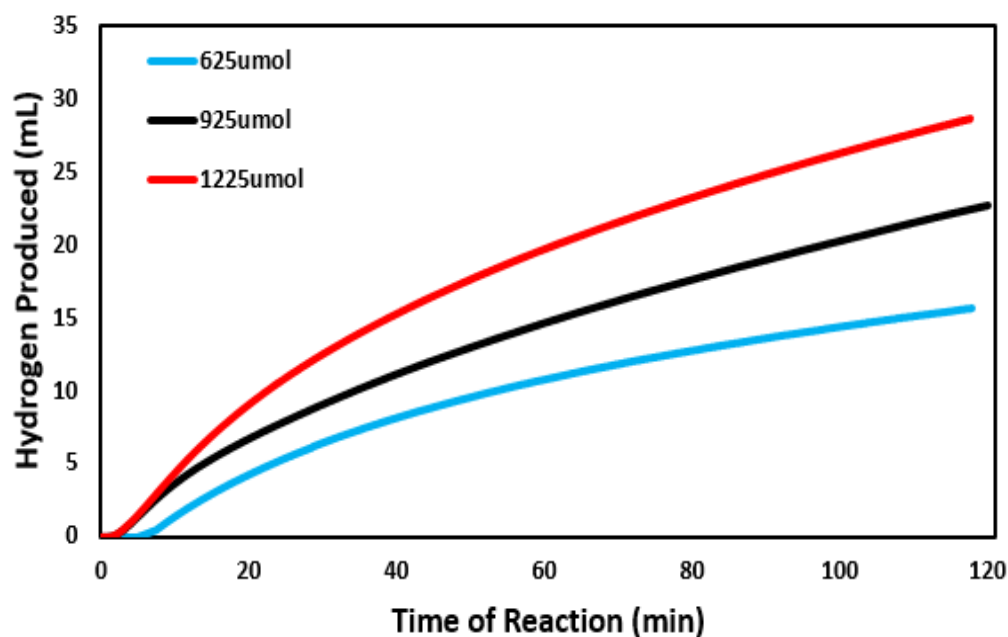
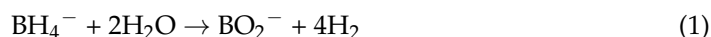


Figure 6. Volume of H_2 generated versus time at varying sodium borohydride concentrations ($625 \mu\text{mol}$, $925 \mu\text{mol}$, $1225 \mu\text{mol}$). Reactions were run at ambient conditions for approximately 120 min.

3.3. Effect of pH on Catalytic Ability

When the reaction was run using solutions of different pH's, the highest rate hydrogen production rate was seen at acidic conditions (pH 6) with a rate of $1.121 \text{ mL min}^{-1} \text{ mL}_{\text{cat}}^{-1}$ (Figure 7). This was then followed by pH 7 and pH 8 with evolution rates of $0.944 \text{ mL min}^{-1} \text{ mL}_{\text{cat}}^{-1}$ and $0.560 \text{ mL min}^{-1} \text{ mL}_{\text{cat}}^{-1}$, respectively. It is known that the formation of borate ions occurs at lower pH, which increases the reaction rate of the uncatalyzed hydrolysis reaction (Equation (1)) [23].

3.4. Activation Energy and Effect of Temperature on Catalytic Ability

Under varied temperatures, palladium nanoparticles produced the most hydrogen at 303 K with a rate of $1.431 \text{ mL min}^{-1} \text{ mL}_{\text{cat}}^{-1}$ (Figure 8). For the 283 K and 288 K temperature conditions, rates of $0.255 \text{ mL min}^{-1} \text{ mL}_{\text{cat}}^{-1}$ and $0.585 \text{ mL min}^{-1} \text{ mL}_{\text{cat}}^{-1}$ were observed, respectively. Finally, a hydrogen generation rate of $0.944 \text{ mL min}^{-1} \text{ mL}_{\text{cat}}^{-1}$ was seen at 295 K (Figure 8). Based on Figure 8 and Equation (2), the activation energy was calculated from the temperature trials to be 58.9 kJ/mol (Figure 9). Palladium nanoparticles displayed a similar activation energy when compared to other catalysts in literature (Table 1). The activation energy of Pd nanoparticles in this study is very attractive compared to most of

the catalysts reported in the literature. In this study, it was conducted in ambient condition in the range of 273 K to 303 K.

$$\ln K = \ln A - E_a/RT \quad (2)$$

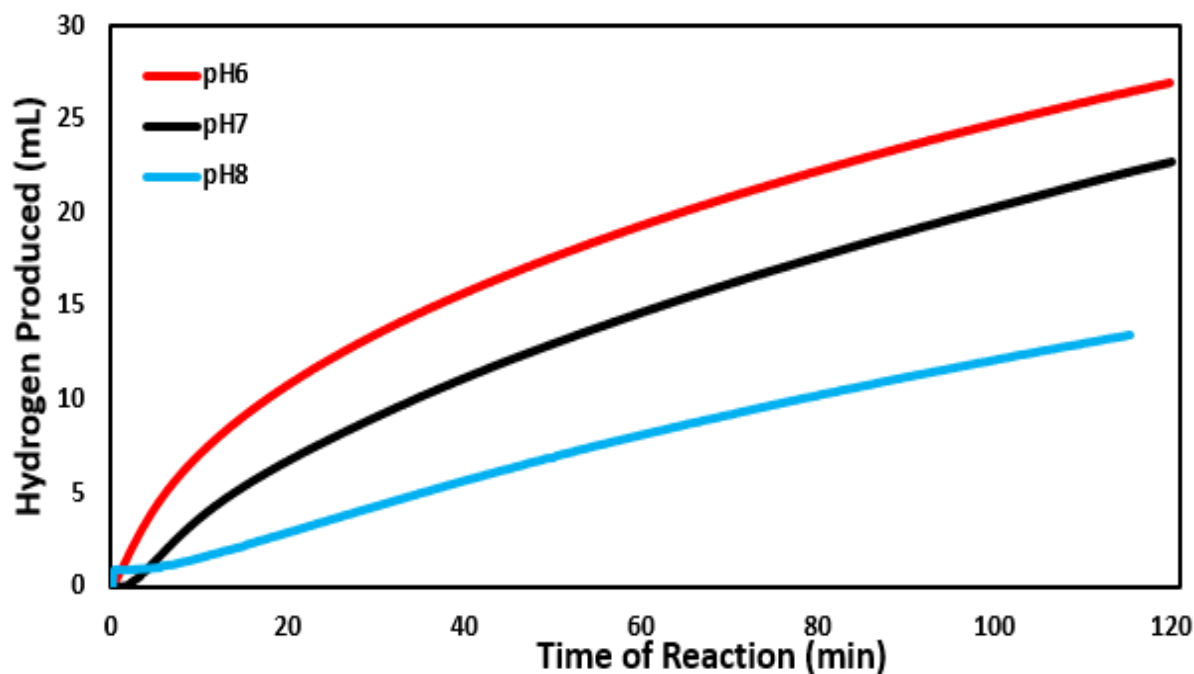


Figure 7. The amount of hydrogen gas produced in mL versus time in minutes as catalyzed by the palladium nanoparticles under varied solution pH's (pH 6, 7, 8). The reactions were run at 295 K with 925 μmol of NaBH_4 for roughly 120 min.

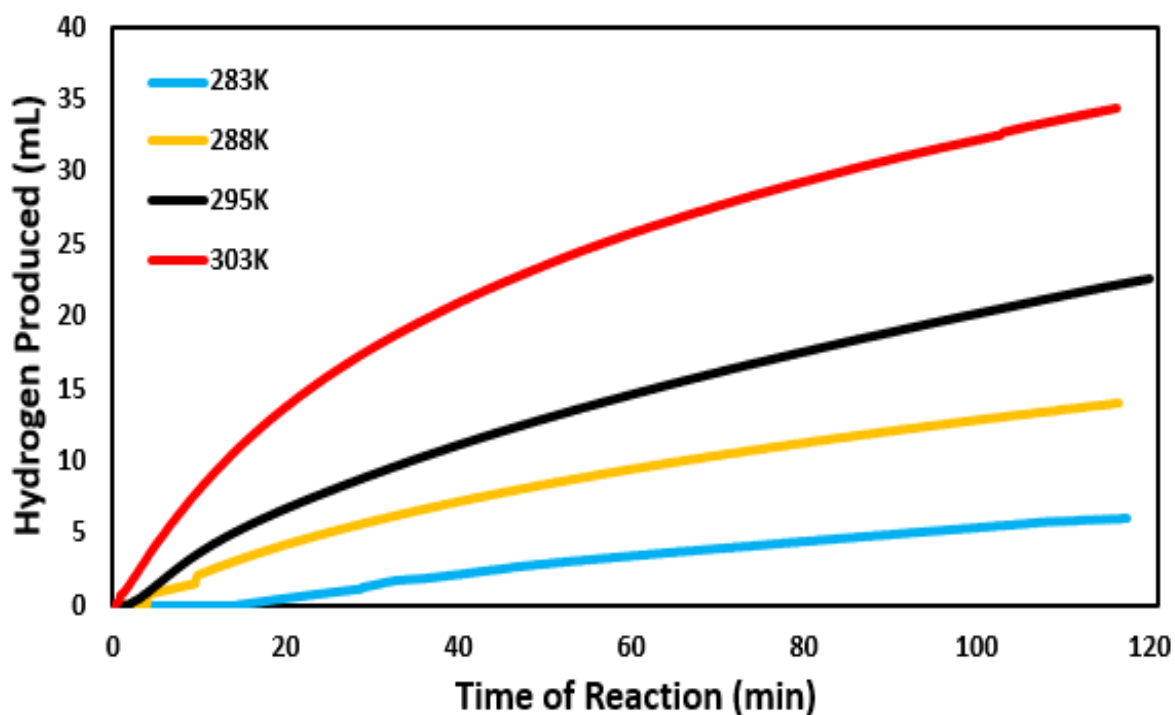


Figure 8. The varied amount of hydrogen produced by the hydrolysis of NaBH_4 versus time as catalyzed by the PdNPs at 283 K, 288 K, 295 K, and 303 K. The reactions conditions included pH 7 and a concentration of 925 μmol of NaBH_4 for upwards of 120 min.

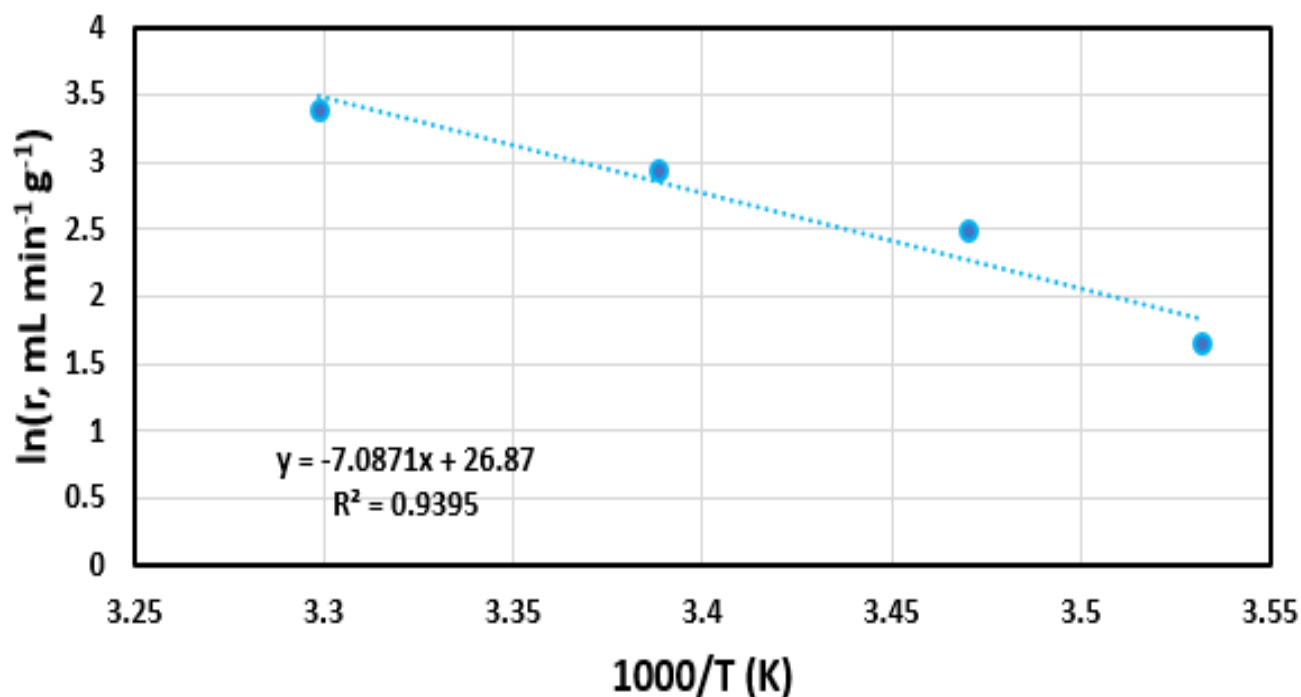


Figure 9. Arrhenius Plot created from the temperature data allowed for the calculation of the activation energy of the NaBH₄ reaction catalyzed by the PdNPs.

Table 1. Reported activation energies for NaBH₄ hydrolysis by catalyst.

Catalyst	E _a (kJ/mol)	T (K)	Reference
AuNPs	54.7	283–303	[10]
Au/MWCNTs	21.1	273–303	[11]
Ag/MWCNTs	44.5	273–303	[12]
Pd/C	28.0	283–323	[16]
Pt-Pd-CNTs	19.0	302–332	[17]
Ru nanoclusters	41.0	298–318	[37]
Ni nanoclusters	54.0	298–318	[38]
Ni-Ru nanoclusters	52.7	288–348	[39]
Co/Fe ₃ O ₄ @C	49.2	288–328	[40]
Co–Cr–B	44.5	293–333	[41]
Cu-Fe-B	57	285–333	[42]
CuNWs	42.5	298–333	[43]
Cu based catalyst	61.2	293–313	[44]
PtMWCNT	46.2	283–303	[45]
PtNPs	39.2	283–303	[46]
AgNPs	50.3	273–303	[47]
PdNPs	58.9	273–303	This Work

Figure 10 depicts the stability of our PdNPs catalyst over the course of five consecutive hydrogen generation trials. Each trial produced similar volumes of hydrogen with an average volume of 32.9 mL observed among all trials. These results show a clear benefit to our catalyst as it can be utilized multiple times without a significant change in productivity.

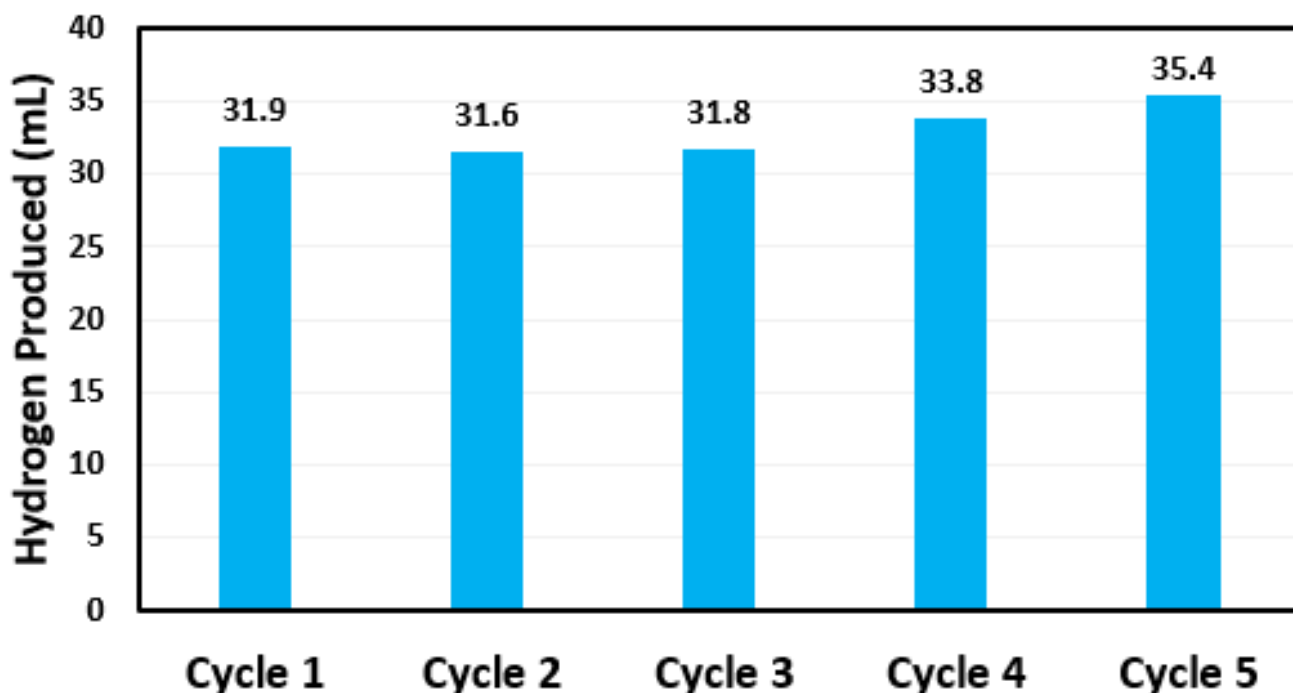
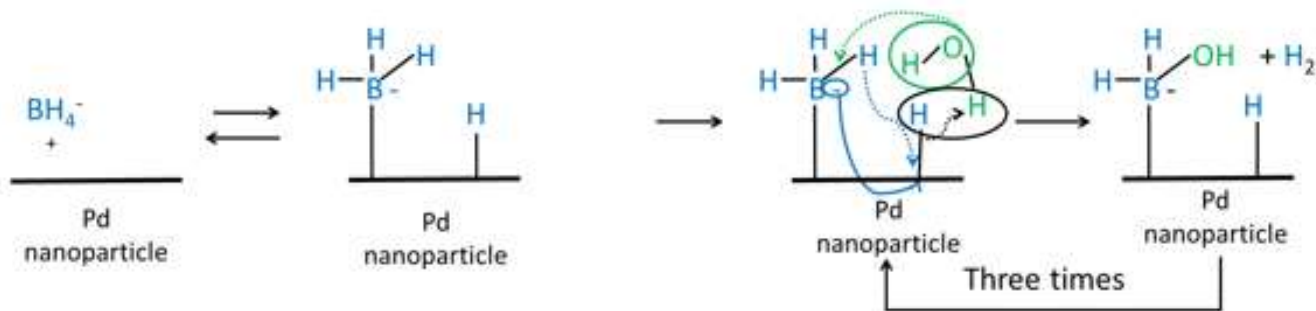
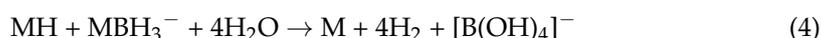


Figure 10. Reusability of the same PdNPs material for the reaction of sodium borohydride in water. Each trial ran for 120 min at 295 K and used 925 μm of NaBH_4 .

Table 1 is based on the Michaelis–Menten model for metal catalyzed hydrolysis of aqueous NaBH_4 (Equations (3) and (4)) [9,11,12,17]. The proposed mechanism and its equations show how both the active catalytic metal site and an adjacent unoccupied site can stabilize the borohydride complex with the metal and the hydride ions. This indicates that the surface area of a catalyst is incredibly important to this reaction as unoccupied metal sites are also shown to aid in catalysis. The Scheme 1 also depicts the multi-electron process of this reaction, in which the last step repeats until tetrahydroxyborate is released from the metal site. Therefore, it is believed that a successful catalyst facilitates the movement of electrons between adjacent sites.



Scheme 1. Our proposal for the mechanism of how sodium borohydride is hydrolyzed by catalysts from the group ten metal nanoparticles.

4. Conclusions

The ultra-small palladium nanoparticles were produced with the assistance of beta-cyclodextrin as organo-nanocup capping agent. The nanoparticles were then characterized

via UV-Vis, TEM, FTIR, and XRD before application as a catalyst in the hydrolysis of sodium borohydride. The resultant ~3 nm Pd nanoparticles performed well as a catalyst with great usability, with an activation energy calculated to be 58.9 kJ/mol. The palladium nanoparticles show promise as a catalyst for application in sodium borohydride-based fuel cells.

Author Contributions: E.B.: data curation, formal analysis, writing—original draft. Q.Q.: data curation, formal analysis, writing—original draft. C.H.: data curation, formal analysis, writing—original draft. T.M.A.-F.: conceptualization, validation, formal analysis, investigation, resources, supervision, writing—review & editing. All authors have read and agreed to the published version of the manuscript.

Funding: This research received no external funding.

Institutional Review Board Statement: Not applicable.

Informed Consent Statement: Not applicable.

Data Availability Statement: The data presented in this study are available on request from the corresponding author.

Acknowledgments: Corresponding Author acknowledges Lawrence J. Sacks Professorship in Chemistry.

Conflicts of Interest: The authors declare no conflict of interest.

References

1. Mahmoud, M.E.; Khalifa, M.; Wakeel, Y.E.; Header, M.; Abdel-Fattah, T.M. Engineered nano-magnetic iron oxide-urea-activated carbon nanolayer sorbent for potential removal of uranium (VI) from aqueous solution. *J. Nucl. Mater.* **2017**, *487*, 13–22. [[CrossRef](#)]
2. Mahmoud, M.E.; Ahmed, S.B.; Osman, M.M.; Abdel-Fattah, T.M. A novel composite of nanomagnetite-immobilized-baker's yeast on the surface of activated carbon for magnetic solid phase extraction of Hg(II). *Fuel* **2015**, *139*, 614–621. [[CrossRef](#)]
3. Ebrahim, S.; Labebe, M.; Abdel-Fattah, T.; Soliman, M. CdTe quantum dots capped with different stabilizing agents for sensing of ochratoxin a. *J. Lumin.* **2017**, *182*, 154–159. [[CrossRef](#)]
4. Dushatinski, T.; Abdel-Fattah, T.M. Carbon nanotube composite mesh films with tunable optoelectronic performance. *ECS J. Solid State Sci. Technol.* **2015**, *4*, M1–M5. [[CrossRef](#)]
5. Abdel-Fattah, T.; Wixtrom, A.; Zhang, K.; Baumgart, H. Highly uniform self-assembly gold nanoparticles over high surface area dense ZnO nanorod arrays as novel surface catalysts. *ECS J. Solid State Sci. Technol.* **2014**, *3*, M61–M64. [[CrossRef](#)]
6. Saad, L.; Feteha, M.Y.; Ebrahim, S.; Soliman, M.; Abdel-Fattah, T. Dye sensitized solar cell based on polyaniline-carbon nanotubes/graphite composite. *ECS J. Solid State Sci. Technol.* **2014**, *3*, M55–M60. [[CrossRef](#)]
7. Abdel-Fattah, T.M.; Wixtrom, A. Catalytic reduction of 4-nitrophenol using gold nanoparticles supported on carbon nanotubes. *ECS J. Solid State Sci. Technol.* **2014**, *3*, M18–M20. [[CrossRef](#)]
8. Ebrahim, S.; El-Raey, R.; Hefnawy, A.; Ibrahim, H.; Soliman, M.; Abdel-Fattah, T.M. Electrochemical sensor based on polyaniline nanofibers/single wall carbon nanotubes composite for detection of malathion. *Synth. Met.* **2014**, *190*, 13–19. [[CrossRef](#)]
9. Huff, C.; Dushatinski, T.; Barzanjii, A.; Abdel-Fattah, N.; Barzanjii, K.; Abdel-Fattah, T.M. Pretreatment of gold nanoparticle multi-walled carbon nanotube composites for catalytic activity toward hydrogen generation reaction. *ECS J. Solid State Sci. Technol.* **2017**, *6*, M69–M71. [[CrossRef](#)]
10. Quach, Q.; Biehler, E.; Elzamzami, A.; Huff, C.; Long, J.M.; Abdel-Fattah, T.M. Catalytic activity of beta-cyclodextrin-gold nanoparticles network in hydrogen evolution reaction. *Catalysts* **2021**, *11*, 118. [[CrossRef](#)]
11. Huff, C.; Dushatinski, T.; Abdel-Fattah, T.M. Gold nanoparticle/multi-walled carbon nanotube composite as novel catalyst for hydrogen evolution reactions. *Int. J. Hydrog. Energy* **2017**, *42*, 18985–18990. [[CrossRef](#)]
12. Huff, C.; Long, J.; Aboulatta, A.; Heyman, A.; Abdel-Fattah, T. Silver nanoparticle/multi-walled carbon nanotube composite as catalyst for hydrogen production. *ECS J. Solid State Sci. Technol.* **2017**, *6*, M115–M118. [[CrossRef](#)]
13. Ye, X.R.; Lin, Y.; Wai, C.M. Decorating catalytic palladium nanoparticles on carbon nanotubes in supercritical carbon dioxide. *Chem. Commun.* **2003**, 642–643. [[CrossRef](#)]
14. Corma, A.; Garcia, H.; Leyva, A. Catalytic activity of palladium supported on single wall carbon nanotubes compared to palladium supported on activated carbon: Study of the Heck and Suzuki couplings, aerobic alcohol oxidation and selective hydrogenation. *J. Mol. Catal. A Chem.* **2005**, *230*, 97–105. [[CrossRef](#)]
15. Li, Y.; Hong, X.M.; Collard, D.M.; El-Sayed, M.A. Suzuki cross-coupling reactions catalyzed by palladium nanoparticles in aqueous solution. *Org. Lett.* **2000**, *2*, 2385–2388. [[CrossRef](#)]
16. Patel, N.; Patton, B.; Zanchetta, C.; Fernandes, R.; Guella, G.; Kale, A.; Miotello, A. Pd-C powder and thin film catalysts for hydrogen production by hydrolysis of sodium borohydride. *Int. J. Hydrog. Energy* **2008**, *33*, 287–292. [[CrossRef](#)]

17. Pena-Alonso, R.; Sicurelli, A.; Callone, E.; Caturan, G.; Raj, R. A picoscale catalyst for hydrogen generation from NaBH₄ for fuel cells. *J. Power Sources* **2007**, *165*, 315–323. [[CrossRef](#)]
18. Chandra, M.; Xu, Q. A high-performance hydrogen generation system: Transition metal-catalyzed dissociation and hydrolysis of ammonia-borane. *J. Power Sources* **2006**, *156*, 190–194. [[CrossRef](#)]
19. Liu, B.; Li, Z. A review: Hydrogen generation from borohydride hydrolysis reaction. *J. Power Sources* **2009**, *187*, 527–534. [[CrossRef](#)]
20. Liu, B.H.; Li, Z.P.; Suda, S. Nickel- and Cobalt-based catalysts for hydrogen generation by hydrolysis of borohydride. *J. Alloys Compd.* **2006**, *415*, 288–293. [[CrossRef](#)]
21. Oezkar, S.; Zahmakiran, M. hydrogen generation from hydrolysis of sodium borohydride using Ru (0) nanoclusters as catalysts. *J. Alloys Compd.* **2005**, *404–406*, 728–731. [[CrossRef](#)]
22. Hua, D.; Hanxi, Y.; Xinping, A.; Chuasin, C. Hydrogen production from catalytic hydrolysis of sodium borohydride solution using nickel boride catalyst. *Int. J. Hydrog. Energy* **2003**, *28*, 1095–1100. [[CrossRef](#)]
23. Schlesinger, H.; Brown, H.; Finholt, A.; Gilbreath, J.; Hoekstra, H.; Hyde, E. Sodium borohydride, its hydrolysis and its use as a reducing agent and in the generation of hydrogen. *J. Am. Chem. Soc.* **1952**, *75*, 215–219. [[CrossRef](#)]
24. Ingersoll, J.; Mani, N.; Thenmozhiyal, J.; Muthaiah, A. A Catalytic Hydrolysis of Sodium Borohydride by a Novel Nickel-cobalt-boride Catalyst. *J. Power Sources* **2007**, *173*, 450–457. [[CrossRef](#)]
25. Shang, Y.; Chen, R.; Jiang, G. Kinetic Study of NaBH₄ Hydrolysis over carbon-supported ruthenium. *Int. J. Hydrog. Energy* **2008**, *33*, 6719–6726. [[CrossRef](#)]
26. Levy, A.; Brown, J.B.; Lyons, C.L. Catalyzed hydrolysis of sodium borohydride. *Ind. Engg. Chem.* **1960**, *3*, 211–214. [[CrossRef](#)]
27. Daniel, M.; Astruc, D. Gold Nanoparticles: Assembly, supramolecular chemistry, quantum-size-related properties, and applications toward biology, catalysis, and nanotechnology. *Chem. Rev.* **2004**, *104*, 293–346. [[CrossRef](#)]
28. Nasrollahzadeh, M.; Sajadi, S.M.; Honarmand, E.; Maham, M. Preparation of palladium nanoparticles using euphorbia thymifolia L. leaf extract and evaluation of catalytic activity in the ligand-free Stille and Hiyama cross-coupling reactions in water. *New J. Chem.* **2015**, *39*, 4745–4752. [[CrossRef](#)]
29. Ramalingam, V.; Raja, S.; Harshavardhan, M. In-situ one step synthesis of polymer functionalized palladium nanoparticles: An efficient anticancer agent against breast cancer. *Dalton Trans.* **2020**, *49*, 3510–3518. [[CrossRef](#)]
30. Shaik, M.R.; Ali, Z.J.Q.; Khan, M.; Kuniyil, M.; Assal, M.E.; Alkhatlan, H.Z.; Al-Warthan, A.; Siddiqui, M.R.H.; Khan, M.; Adil, S.F. Green synthesis and characterization of palladium nanoparticles using origanum vulgare L. extract and their catalytic activity. *Molecules* **2017**, *22*, 165. [[CrossRef](#)]
31. Szejtli, J. Introduction and General Overview of Cyclodextrin Chemistry. *Chem. Rev.* **1998**, *98*, 1743–1754. [[CrossRef](#)]
32. Chi, T.T.K.; Le, N.T.; Hien, B.T.T.; Trung, D.Q.; Liem, N.Q. Preparation of SERS substrates for the detection of organic molecules at low concentration. *Commun. Phys.* **2016**, *26*, 261–268. [[CrossRef](#)]
33. Vorontsov, A.V.; Tsybulya, S.V. Influence of nanoparticles size on XRD Patterns for small Monodisperse nanoparticles of Cu₀ and TiO₂ anatase. *Ind. Eng. Chem. Res.* **2018**, *57*, 2526–2536. [[CrossRef](#)]
34. Navaladian, S.; Viswanathan, B.; Varadarajan, T.K.; Viswanath, R.P. A rapid synthesis of oriented palladium nanoparticles by UV irradiation. *Nanoscale Res. Lett.* **2009**, *4*, 181–186. [[CrossRef](#)]
35. Song, Y.; Kumar, C.S.S.R.; Hormes, J. Synthesis of palladium nanoparticles using a continuous flow polymeric micro reactor. *J. Nanosci. Nanotech.* **2004**, *4*, 788–793. [[CrossRef](#)]
36. Mahmood, A.; Ahmad, M.; Sarfraz, R.M.; Minhas, M.U. β-CD based hydrogel microparticulate system to improve the solubility of acyclovir: Optimization through in-vitro, in-vivo and toxicological evaluation. *J. Drug Deliv. Sci. Technol.* **2016**, *36*, 75–88. [[CrossRef](#)]
37. Zahmakiran, M.; Ozkar, M. Water dispersible acetate stabilized ruthenium (0) nanoclusters as catalyst for hydrogen generation reaction of sodium borohydride. *J. Mol. Catal.* **2006**, *258*, 95–103. [[CrossRef](#)]
38. Metin, O.; Ozkar, S. Hydrogen generation from the hydrolysis of sodium borohydride by using water dispersible, hydrogen phosphate-stabilized nickel (0) nanoclusters as catalyst. *Int. J. Hydrog. Energy* **2007**, *32*, 1707–1715. [[CrossRef](#)]
39. Liu, C.H.; Chen, B.H.; Hsueh, C.L.; Ku, J.R.; Jeng, M.S.; Tsau, F. Hydrogen generation from hydrolysis of sodium borohydride using Ni-Ru nanocomposite as catalysts. *Int. J. Hydrog. Energy* **2009**, *34*, 2153–2163. [[CrossRef](#)]
40. Chen, B.; Chen, S.; Bandal, H.A.; Appiah-Ntiamoah, R.; Jadhav, A.R.; Kim, H. Cobalt nanoparticles supported on magnetic core-shell structured carbon as a highly efficient catalyst for hydrogen generation from NaBH₄ hydrolysis. *Int. J. Hydrog. Energy* **2018**, *43*, 9296–9306. [[CrossRef](#)]
41. Chen, Y.; Jin, H. Fabrication of amorphous Co–Cr–B and catalytic sodium borohydride hydrolysis for hydrogen generation. *J. Mater. Res.* **2020**, *35*, 281–288. [[CrossRef](#)]
42. Loghmani, M.H.; Shojaei, A.F.; Khakzad, M. Hydrogen generation as a clean energy through hydrolysis of sodium borohydride over Cu-Fe-B nano powders: Effect of polymers and surfactants. *Energy* **2017**, *126*, 830–840. [[CrossRef](#)]
43. Hashimi, A.S.; Nohan, M.A.; Chin, S.X.; Khiew, P.S. Copper Nanowires as Highly Efficient and Recyclable Catalyst for Rapid Hydrogen Generation from Hydrolysis of Sodium Borohydride. *Nanomaterials* **2020**, *10*, 1153. [[CrossRef](#)]
44. Balbay, A.; Saka, C. Effect of phosphoric acid addition on the hydrogen production from hydrolysis of NaBH₄ with Cu based catalyst. *Energy Sources Part A Recovery Util. Environ. Eff.* **2018**, *40*, 794–804. [[CrossRef](#)]

45. Huff, C.; Quach, Q.; Long, J.M.; Abdel-Fattah, T.M. Nanocomposite catalyst derived from ultrafine platinum nanoparticles and carbon nanotubes for hydrogen generation. *ECS J. Solid State Sci. Technol.* **2020**, *9*, 101008. [[CrossRef](#)]
46. Huff, C.; Biehler, E.; Quach, Q.; Long, J.M.; Abdel-Fattah, T.M. Synthesis of highly dispersive platinum nanoparticles and their application in a hydrogen generation reaction. *Colloids Surf. A Physicochem. Eng. Asp.* **2020**, *610*, 125734. [[CrossRef](#)]
47. Huff, C.; Long, J.M.; Abdel-Fattah, T.M. Beta-cyclodextrin-assisted synthesis of silver nanoparticle network and its application in a hydrogen generation reaction. *Catalyst* **2020**, *10*, 1014. [[CrossRef](#)]